ACS APPLIED MATERIALS & INTERFACES

Research Article

www.acsami.org

Nanostructural Characteristics and Interfacial Properties of Polymer Fibers in Cement Matrix

Faezeh Shalchy

Department of Civil and Environmental Engineering Worcester Polytechnic Institute, Worcester, Massachusetts 01609, United States

Nima Rahbar*

Department of Civil and Environmental Engineering Worcester Polytechnic Institute, Worcester, Massachusetts 01609, United States

ABSTRACT: Concrete is the most used material in the world. It is also one of the most versatile yet complex materials that humans have used for construction. However, an important weakness of concrete (cement-based composites) is its low tensile properties. Therefore, over the past 30 years many studies were focused on improving its tensile properties using a variety of physical and chemical methods. One of the most successful attempts is to use polymer fibers in the structure of concrete to obtain a composite with high tensile strength and ductility. The advantages of polymer fiber as reinforcing material in concrete, both with regard to reducing environmental pollution and the positive effects on a country's economy, are beyond dispute. However, a thorough understanding of the mechanical behavior of fiber-reinforced concrete requires a knowledge of fiber/matrix interfaces at the nanoscale. In this study, a combination of atomistic simulations and experimental techniques has been used to study the nanostructure of fiber/matrix interfaces. A new model for calcium−silicate−hydrate (C−S−H)/fiber interfaces is also proposed on the basis of scanning electron microscopy (SEM) and energy-dispersive X-ray spectroscopy (EDX) analyses. Finally, the adhesion energy between the C−S−H gel and three different polymeric fibers (poly(vinyl alcohol), nylon-6, and polypropylene) were numerically studied at the atomistic level because adhesion plays a key role in the design of ductile fiber-reinforced composites. The mechanisms of adhesion as a function of the nanostructure of fiber/matrix interfaces are further studied and discussed. It is observed that the functional group in the structure of polymer macromolecule affects the adhesion energy primarily by changing the C/S ratio of the C−S−H at the interface and by absorbing additional positive ions in the C−S−H structure.

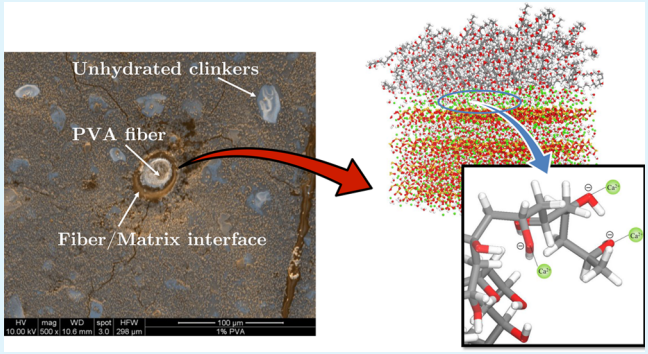

KEYWORDS: *concrete, molecular dynamics, fiber/matrix interface, EDX analysis, polymeric fibers*

1. INTRODUCTION

As the most used material in the world, concrete possesses excellent compressive strength but weak tensile properties. The cement-based matrix of the concrete has a complex structure that makes concrete a weak material in terms of material properties such as tensile strength and toughness. Therefore, over the past 30 years many studies were focused on improving the tensile properties of concrete (cement-based composites) using a variety of physical and chemical methods.[1−4] One of the most successful attempts is to use polymeric materials in the structure of concrete to obtain a composite with high tensile strength and ductility.[5−8] Improving the performance of polymer-fiber-reinforced cement composites can also increase the durability of concrete structures and decrease the production of carbon dioxide.[9,10] However, understanding the mechanical behavior of fiber-reinforced concrete requires a thorough knowledge of the fiber/matrix interface structure. Although a large body of microscopic studies have been carried out on the interfaces present in fiber-reinforced cement-based composites,[8,11,12] the nanostructure of interfaces between cement and polymer fiber has not been thoroughly investigated.[8,11,12] This understanding is needed to fully predict and improve the mechanical properties of fiber-reinforced cement-based composites.[8,11,12]

This paper presents a combined experimental and numerical study on the nanostructural properties of polymer/cement interfaces. The atomistic structure of the principal hydration product of Portland cement, calcium silicate hydrate, C−S−H (C: CaO, S: SiO_2, and H: H_2O) is first modeled using molecular dynamics (MD) and is verified by the available experimental data. In Portland cement, the raw materials are limestone and clay. Hence, a typical composition of a clinker is about 67% CaO and 22% SiO_2, with mainly alite (C_3S) and belite (C_2S) molecules. The products of the hydration reaction

Received: May 19, 2015
Accepted: July 27, 2015
Published: July 27, 2015

DOI: 10.1021/acsami.5b04344
ACS Appl. Mater. Interfaces 2015, 7, 17278−17286

of clinker are mainly portlandite (CH) and C−S−H gel. The C−S−H gel makes up to 70% of the final volume and is responsible for the cohesion and strong mechanical properties of cement pastes.[13]

During the past decade, the principal new data bearing on the structure of polymer/cement interface have been on compositions, determined by X-ray microanalysis, and on silicate anion structures.[14,15] Emphasis is placed on some recent models and their ability to account for these data. There are also many experimental studies on C−S−H gel structure. In a study by Uzun et al.,[15] X-ray diffraction (XRD) is used to investigate the atomistic structure of C−S−H considering the coordinate number of Ca−O. They believed that C−S−H is an evolution of a tobermorite-like structure to a jennite-like structure. Allen et al.[16] measured the mean formula and solid density of the nanoscale C−S−H gel particles by combining small-angle neutron and X-ray scattering data ($(CaO)_{1.7}(SiO_2)$-$(H_2O)_{1.8}$ and d = 2.604 mg/m^3).

An understanding of the nature of chemical reactions occurring in C−S−H is also necessary in modeling the mechanical properties of concrete at nanoscale. To understand the chemical reactions in C−S−H, many researchers have previously tried to characterize the structure of C−S−H gel at the atomistic level.[17−21] In that regard, different strategies were utilized to model the atomistic structure of C−S−H in order to understand its nanostructure properties.[22,23] Bauchy et al. constructed the tobermorite crystalline structure, a more realistic C−S−H, and an artificial ideal glass.[24] They showed that although C−S−H retains some signatures of a tobermorite-like layered structure hydrated species are completely amorphous nitrogen. Earlier, Pellenq et al.[25] proposed a molecular model for C−S−H gel with the stoichiometry of $(CaO)_{1.65}(SiO_2)(H_2O)_{1.73}$. In a more recent study, Qomi et al. investigated the effect of C/S ratio on the molecular structure of C−S−H using MD simulation technique.[26]

The adhesion energy between fiber and matrix plays a vital role in the mechanical properties of composites.[11] In this paper, we have carried out SEM and EDX analysis techniques to create a new atomistic model for C−S−H gel and its interface with polymeric materials. The proposed model is studied and analyzed by MD simulation using ab initio based force fields. The resulting nanostructure of C−S−H using the proposed model is validated by available nuclear magnetic resonance (NMR) spectroscopy data. Finally, the molecular adhesion mechanisms between a layered structure of C−S−H gel and three different polymeric fibers with a variety of polarities are investigated, and the mechanisms of adhesion are reported.

2. MATERIALS AND METHODS

2.1. Experimental Methods. In this study, we primarily propose a more realistic molecular model for the complex C−S−H gel, particularly at the fiber/matrix interface, with the help of SEM/EDX analysis. Using this molecular model, we then proceed to investigate the adhesion energies between proposed model of C−S−H gel and three different polymeric fibers to understand the overall behavior of polymer/cement composites. The first two polymer fibers, PVA and nylon-6 with the IUPAC names of poly(vinyl alcohol) and poly(hexano-6-lactam), respectively, have polar side chains with different polarities. The third polymer fiber is polypropylene, which has a nonpolar side chain. The goal is to observe how the polarity of the side chains affects the nanostructure of fiber/cement interface.

2.1.1. Polymer Fibers Characteristics. In this study, three different polymer fibers are considered on the basis of the polarities of their side chains. The same functional group usually undergoes the same or similar chemical reaction(s) regardless of the size of its molecule.[27]

Nylon-6 has amide groups (Figure 1a), which have the highest polarities among other functional groups. It has two different highly

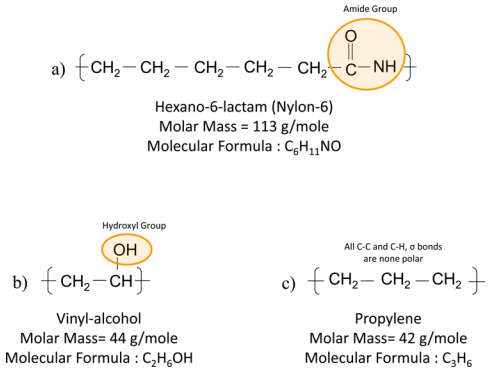

Figure 1. Monomer formula for three different polymers used as fibers in cement paste are shown in this picture: (a) monomer for nylon-6, (b) monomer of PVA, and (c) monomer of polypropylene. It can be observed that nylon-6 has an amide side chain on its monomer, whereas PVA has hydroxyl groups. Polypropylene's macromolecule is mainly nonpolar.

electronegative atoms in its structure: oxygen and nitrogen atoms in the amide group. Both oxygen and nitrogen contribute to hydrogen bonding. Nitrogen atoms are hydrogen-bond acceptors and/or donors, and oxygen atoms are hydrogen-bond acceptors. PVA is one of the most common fibers that have been used in fiber-reinforced cement composites. PVA is from the alcohol group that has a hydroxyl side chain (Figure 1b). On one hand, this functional group has less polarity than amide group; on the other hand, the alcoholic functional group has just one oxygen atom that contributes to hydrogen bonding. Oxygen atoms in the hydroxyl group are hydrogen-bond acceptors and/or donors. The last polymer, polypropylene, is composed of alkanes (Figure 1c). Alkanes have little intermolecular association because the carbon−hydrogen bond is nonpolar. Alkanes are essentially nonpolar molecules and are insoluble in water. All of the fibers were provided by Forta Corporation Company (Grove City, PA).

2.1.2. Fiber-Reinforced Cement Paste. The fiber-reinforced cement paste composites evaluated in this study are prepared by mixing polymer fibers, water, and cement powder to obtain mixtures with a specific concentration of fibers for a specific composition of cement.

The cement paste ingredients are mixed with a blender. All samples have 1 wt % of polymeric fibers. The following procedure is used for the preparation of the cement pastes: First, the weight percentage of cement, fiber, and water are measured in different bowls. Second, the cement is mixed at a medium speed for 15 s; water and fibers are added to the cement gradually and they are mixed for 90 s. A spatula is used to scrape the wall and bottom of the bowl; Another 90 s of mixing is done at medium speed. After the mixing is complete, the fresh cement pastes are cast in plastic cylinders with a 5.1 cm diameter and 10.2 cm height and are sealed at 23 ± 1 °C for curing in a curing room. At the age of 24 ± 1 h, the cylinder samples are demolded. Any excess of moisture on the surface is removed with a towel, and the specimens are sealed in plastic bags at 23 ± 1 °C until the age of testing. To ensure desired compressive strength, the samples are tested after 28 days, then cut using a diamond cutter and polished for the SEM/EDX analysis.

2.1.3. SEM/EDX Analysis. A typical SEM image of the polymer fiber, matrix, and polymer−matrix interfacial transition zones for all three types of polymer fibers is shown in Figure 2. The SEM images of the samples clearly show that there is a transition zone between the polymer fibers and cement paste. These figures show that the interfacial layer between fiber and matrix has a thickness of about 1−5

DOI: 10.1021/acsami.5b04344
ACS Appl. Mater. Interfaces 2015, 7, 17278−17286

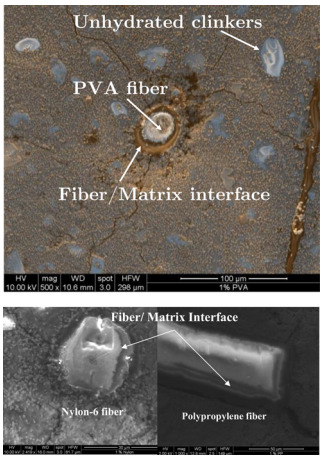

Figure 2. SEM images of fiber/matrix interface for PVA (top), nylon-6 (bottom left), and polypropylene (bottom right). Regions of fiber/matrix interface are indicated in the image.

μm around the fiber. Regions of fiber, cement matrix, unhydrated clinkers, and fiber/matrix interface are also indicated in the figure.

The EDX results and analysis for three different fiber/cement interfaces are shown in Figure 3. X-ray mapping is used to investigate the distribution and density of existing elements such as Si and Ca in an area around each fiber. The X-ray mapping of Si and Ca elements for nylon-6 and PVA fibers clearly show the accumulation of calcium at the fiber/matrix interface, which is represented by a circle on the figures. However, this phenomenon is not observed in the samples with nonpolar polypropylene fibers. Moreover, the EDX is carried out on 10 spectra of the fiber/matrix interface and 10 spectra of regular C−S−H gel. The numerical EDX results show that the ratio of C/S in the interfacial zone significantly changes for PVA and nylon-6 fibers whereas it remains almost constant for polypropylene fibers as shown in Figure 3. The ratio of C/S in the interfacial transition zone between PVA and cement and between nylon-6 fibers and cement increases in comparison to that of the regular C−S−H in fiber-reinforced composite matrices. Furthermore, this ratio does not change for the polypropylene fibers. This may be due to the polarity of different fibers caused by the functional groups on their molecular structure.

2.2. Atomistic Simulations. To have a better understanding of C−S−H at nanoscale, Taylor's postulate is used to begin atomistic modeling.[18] C−S−H gel is mostly made of tobermorite and jennite.[23] Tobermorite has the chemical formulation of $Ca_5Si_6O_{16}(OH)_2{\cdot}7H_20$ with a C/S ratio of 0.83 and density of 2.18 g/cm^3, whereas Jennite has the chemical formulation of $Ca_9(Si_6O_{18})$ $(OH)_6{\cdot}8H_2O$ with a C/S ratio of 1.5 and density of 2.27 g/cm^3. Moreover, the C/S ratio in C−S−H varies from 0.7 to 2.3, and its density is about 2.6 g/cm^3.[25] Using this information, a more realistic model for C−S−H is proposed in the following sections.

2.2.1. Force Field and Simulation Parameters. The selection of a force field that results in an accurate model for the potential energy hypersurface in which the nuclei moves is an important step in performing atomistic simulations. In general, the potential energy consists of valence, cross-term, and nonbonded energies:[28]

$$E_{\text{total}} = E_{\text{valence}} + E_{\text{cross-term}} + E_{\text{nonbonded}} \quad (1)$$

In eq 1, a bond-stretching term, a bending energy term, and four body terms, including a dihedral-bond−torsion-angle term and an inversion (out-of-plane interaction) term have contribution to the valence energy. The cross-term enegy, $E_{\text{cross-term}}$, accounts for the energy induced by the changes in the bond length and the bond angle with the surrounding atoms. $E_{\text{nonbonded}}$, the nonbonded term, consists of intermolecular and intramolecular interaction. The nonbonded terms include hydrogen bonds (H bonds) and van der Waals (vdW) interactions that are the induced dipole−dipole interaction (also known as London forces). Moreover, the Coulomb interactions

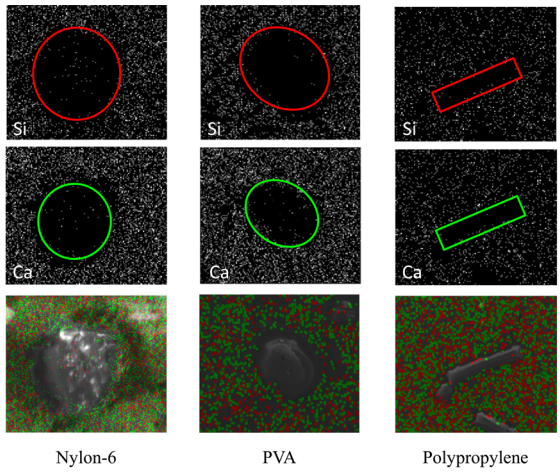

(a)

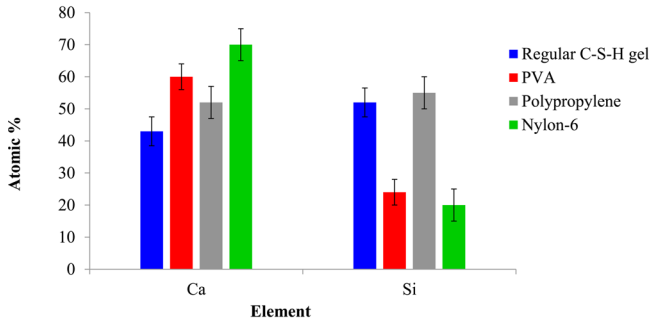

(b)

Figure 3. (a) EDX X-ray map results for three polymeric fibers in C−S−H matrix. The green dots represent calcium and the red dots represent silicon. The results shows that the Ca^{2+} ions are absorbed on the interface of nylon-6 and PVA fibers, but the interface of polypropylene fiber has not significantly changed. (b) Comparison of the EDX results on samples of regular C−S−H gels and EDX results on samples of polymer/C−S−H gel interfaces. A total of 10 EDX spectra are used for each sample.

account for electrostatic interaction. These are summarized in eqs 2−4.

$$E_{\text{valence}} = E_{\text{stretching}} + E_{\text{bending}} + E_{\text{dihedral-torsion}} + E_{\text{inversion}} \quad (2)$$

$$E_{\text{cross-term}} = E_{\text{bond-bond}} + E_{\text{angle-angle}} + E_{\text{bond-angle}} + E_{\text{end bond-torsion}} + E_{\text{middle bond-torsion}} + E_{\text{angle-torsion}} + E_{\text{angle-angle-torsion}} \quad (3)$$

$$E_{\text{nonbonded}} = E_{\text{vdW}} + E_{\text{Coulomb}} + E_{\text{Hbond}} \quad (4)$$

The COMPASS (condensed-phase optimized molecular potentials for atomistic simulation studies)[29] force field is used for this calculation. It is a powerful force field for atomistic simulation of condensed materials and one of the first ab initio based force fields that is parametrized and validated with the experiment results.[29] Therefore, it is an accurate and reliable force field for predicting mechanical, structural, and thermodynamic properties of vast range of molecules and atoms.[30] It is well-parametrized for nonbonded interaction, which makes it a particularly good fit for long-chain molecules such as biomaterials or polymers and other systems where the vdW interaction is the governing interaction.[31]

DOI: 10.1021/acsami.5b04344
ACS Appl. Mater. Interfaces 2015, 7, 17278−17286

Hence, MD simulations are utilized to understand the nanomechanical proprieties of the interface. The unit cell of C−S−H gel and polymer are created and optimized separately. The simulations are carried out at room temperature. The effects of ambient temperature on the structure of interfaces are not studied because the experiments are done at room temperature after curing. However, the process of cement hydration is exothermic, i.e., it generates heat, but this is during the hydration process in the first 24 h. Here, the atomistic modeling is carried out to simulate the C−S−H/polymer interaction after the hydration reaction. In this step, the temperature can be assumed to be constant around room temperature (298 K).

2.2.2. Atomistic Modeling of C−S−H gel. In this study, the structure of jennite proposed by Hamid[17] is used to initiate the basic molecular model of C−S−H. However, in our model, it is assumed that the interlayer Ca^{2+} ions react with water and produce hydroxyl ions. Hence, the structure that is proposed here is made of SiO_2, Ca^{2+}, and $Ca(OH)_2$ layers arranged as shown in Figure 4a. Afterward, multiple Si atoms are randomly omitted, and multiple Ca^{2+} atoms are added to the structure for the following reasons: (1) to be able to satisfy the C/S ratio in the C−S−H structure at the interface with different polymer fibers, (2) to satisfy the overall charge balance in the system, and (3) to provide the necessary defects in the structure of C−S−H. This approach can be applied to construct different C−S−H models with different C/S ratios using the EDX analysis results.

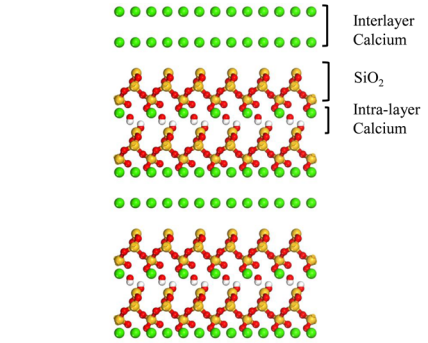

(a)

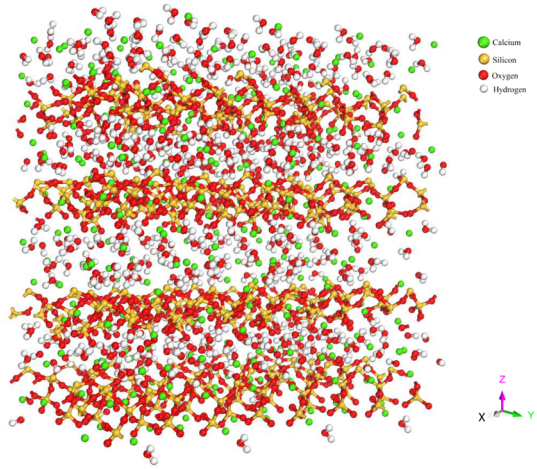

(b)

Figure 4. (a) Schematic of the initial molecular model of C−S−H. (b) Molecular model of C−S−H after optimization. Red and white spheres are oxygen and hydrogen atoms of water molecules, respectively; the green spheres are calcium ions. Yellow and red sticks are silicon and oxygen atoms, respectively, in silica tetrahedra.

Using the steepest descent approach followed by the conjugate gradient method, the layered structure of the C−S−H surface is modeled, and the potential energy is optimized. The dimensions of the system are 40 Å × 40 Å × 45 Å. The charge distribution is calculated using the Qeq method.[32] The nonbonded summations are calculated using Ewald for electrostatic interaction with accuracy of 0.001 kcal/mol. On the basis of each atom's charge with the truncation of atoms further than cutoff distance of 15.5 Å, the charge distribution for van der Waals interaction is computed (Figure 4b).

The thermodynamic properties of the C−S−H are then obtained to assess the suitability of the force field to model the C−S−H gel. The density of C−S−H from the MD and experiments are estimated to be about 2.410 and 2.64 g/cm^3, respectively. The modulus of elasticity is estimated to be 57.02, 24.5231, and 22.20 GPa in *X*, *Y*, and *Z* directions, respectively (Figure 4). Two different methods are used to calculate the elastic moduli. In the first method, the structure is stretched in all three directions, and virial stresses are computed. The Young's modulus is then computed as the average of the three initial stress−strain slopes after relaxation. In the second method, Young's modulus are indirectly computed from MD simulation for each direction by the following equation:

$$\frac{U}{A \times L} = E\frac{1}{2}\left(\frac{L - L_0}{L_0}\right) \tag{5}$$

where L_0 is the initial length of unit cell in desired direction, L is the final length, and U is the energy of the system after increasing the length. It is observed that both methods result in almost the same value for the suggested C−S−H model. The experimental values corresponding to these properties depend on the volume fraction of the porosities and vary from 30 to 50 GPa.[33,34] The Poisson's ratio of C−S−H is also a function of the volume fraction of porosities and changes from 0.15 to 0.3.[18,35] This property is estimated to be 0.29 from the MD simulations using the prescribed force field.

2.2.3. Modeling of the Polymer Fibers. Monomers of the chosen polymers (vinyl alcohol, propylene, and hexano-6-lactam) are constructed, and the molecular structures are presented in Figure 5a−c. Chains of PVA, polypropylene, and nylon-6 are then created by assembling 100 monomer units of vinyl alcohol, propylene, and hexano-6-lactam, respectively.[36] The structure of the PVA, polypropylene, and nylon-6 unit cells are presented in Figure 5d−f. The number of monomers in the chain is obviously not representative of the actual polymer chain because the real chain is composed of more than 10 000 repeating units. However, this length is sufficient to model the chain ends close to the surface. Many monomers on the real chain do not participate in the adhesion process because long-range nonbonded interactions are negligible for these monomers. Chains of 300 monomers and 100 monomers are analyzed, and the properties are found to be similar. Hence, for modeling each polymer, 5 chains of 100 monomers are used to simulate the material properties. Additionally, this length is higher than persistent length of these systems. The persistent length of the polymers investigated in this study is roughly around 5−12 nm. This parameter can be estimated using the following equation:

$$P = \frac{B_s}{k_B T} \tag{6}$$

where $B_s = EI$, with E being the Young's modulus of the polymer and $I = (\pi r^4/4)$ where r is the radius of molecule's cross section. k_B is the Boltzmann constant. Hence, the persistent length parameter for PVA can be estimated as 7.1 nm. The chain length in our models is around 20 nm, which is greater than the persistence length. Moreover, to be able to compute the adhesion energy between C−S−H and the polymers, shorter chains, in which the effect of unfolding of chains, intramolecular interactions, or self-adhesion can be neglected, are preferable.[37] Five possible structures of each prescribed polymer molecule with a desired density of 1.2 g/cm^3 at 298 K are created and optimized. Each configuration is subjected to MD simulation to let the atoms relax down to the minimum energy in the structure.[38] Initially, the canonical (NVT) dynamics is carried out for 60 ps by 1.0

DOI: 10.1021/acsami.5b04344
ACS Appl. Mater. Interfaces 2015, 7, 17278−17286

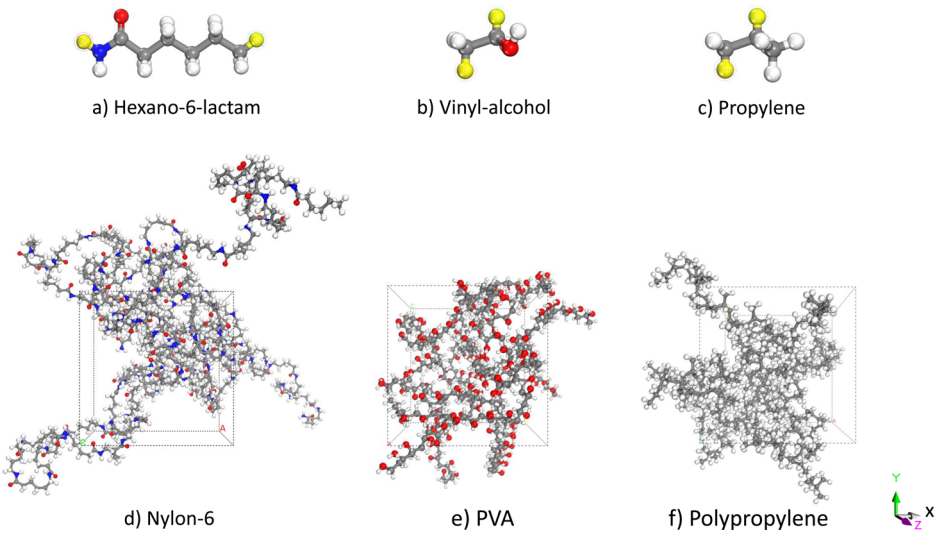

Figure 5. Atomistic models of three different polymer atoms investigated in this study. (a–c) Monomer of nylon-6, PVA, and polypropylene, respectively. Gray, red, white, and blue spheres represent carbon, oxygen, hydrogen, and nitrogen, respectively. Yellow atoms show where the monomer is connected to the other monomers in the polymer chain. These locations will be replaced by hydrogen at the beginning and at the end of each chain. (d–f) Bulk molecular representations in atomistic simulation of nylon-6, PVA, and polypropylene models, respectively.

fs time steps at 300 K, followed by the isothermal–isobaric (NPT) dynamics compressed at high pressure (5000 bar) for 120 ps at 300 K. Next, NVT MD are applied at 600 and 300 K, successively, for about 50 and 70 ps, respectively. Subsequently, 120 ps MD is carried out in the NPT ensemble at 1 bar, and the resulting density is compared to the experimental value. If the density is lower than the experimental density, then the first two steps are repeated. Finally, MD simulation is carried out in NVT ensemble at 1 bar for 300 ps. The simulation results of the density for each polymer are presented in Table 1. The

Table 1. Density (g/cm^3) Values of PVA, Polypropylene, and Nylon-6 Obtained from Atomistic Simulations and Available Experimental Data

material	simulation	experiment
PVA	1.13	1.1[43]
polypropylene	0.84	0.952[44]
nylon-6	1.10	1.13[45]

computed densities are close to available experimental data. Additionally, in order to verify the structure of the polymers, the convergence of root mean square deviations (RMSDs) are also checked.

Young's modulus is a measure of the stiffness of an elastic material. Using MD simulations, this parameter is found by eq 5 for each polymer. Young's moduli of PVA, polypropylene, and nylon-6 computed from the stiffness matrices are presented in Table 2. The average Young's moduli of polymers are in good agreement with the respective experimental measurements.

The glass transition temperature (T_g) is the reversible transition in amorphous materials from a hard and relatively brittle state into a molten or rubberlike state. From a thermodynamic point of view, the glass transition temperature appears as a change in the slope of the

Table 2. Young's Moduli (GPa) of PVA, Polypropylene, and Nylon-6 Obtained from Atomistic Simulations and Available Experimental Data

material	simulation	experiment
PVA	1.4711	2–4[46]
polypropylene	2.42	1.1–1.5[47]
nylon-6	3.72	1.2–2.8[48,49]

specific volume and energy versus temperature.[39] The glass transition temperature (T_g) is obtained from the change in the slope of specific energy–temperature curve.[38,40] To achieve this, the temperature of each system is increased to 600 K and slowly brought down to 200 K at a rate of 0.5 K/ps while the temperature and pressure are controlled by the Nose thermostat and Berendsen barostat, respectively. In random steps, the system is equilibrated with NPT dynamics for 25 ps, and the results are recorded to create the specific energy–temperature curves. The variation of the specific energy with temperature for nylon-6 is presented in the Figure 6. As expected, linear variations are observed on both sides of a critical temperature. This critical temperature should correspond to the glass transition temperature.

The glass transition temperatures of nylon-6, PVA, and polypropylene were computed and compared with the experimental results in Table 3. The small difference between experimental and simulation results is due to the fact that this value will strongly depend on the time scale at which the measurements are carried out.

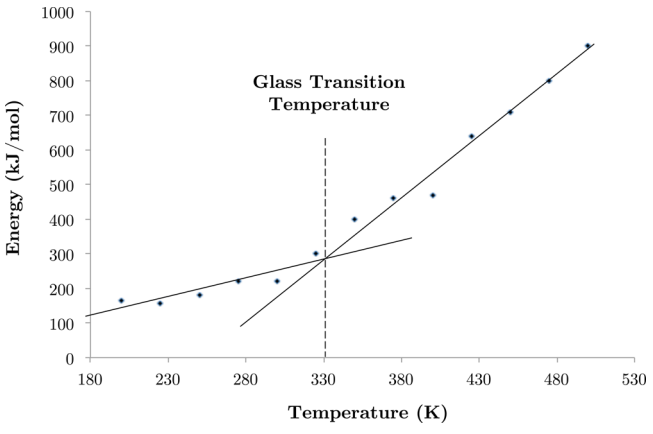

Figure 6. Variation of the specific energy as a function of temperature for nylon-6. The glass transition temperature is obtained from the change in the slope of specific energy–temperature curve. To achieve this, the temperature of each system is increased to 600 K and slowly brought down to 200 K at a rate of 0.5 K/ps while the temperature and pressure are controlled by the Nose thermostat and Berendsen barostat, respectively.

DOI: 10.1021/acsami.5b04344
ACS Appl. Mater. Interfaces 2015, 7, 17278–17286

Table 3. Glass Transition Temperatures (°C) of PVA, Polypropylene, Nylon-6 Obtained from Atomistic Simulations and Available Experimental Data

material	simulation	experiment
PVA	92.4	87[50]
polypropylene	16.7	25−20[43]
nylon-6	58.1	49[43]

2.2.4. Interaction Energy between C−S−H and Polymer Fibers. To measure the adhesion energies between the polymers and C−S−H gel, models are constructed by placing polymer chains on the C−S−H surface models in a supercell. When the polymer is placed on top of the layered structure, the polymer will be able to "see" both sides of the surface because of periodic boundary conditions. Therefore, a large vacuum (50 Å) should be added above the polymer so that it can interact only with one side of the surface. Five different configurations of each chain of polymer are chosen as a confined layer on top of the C−S−H gel. Then, the polymer layers are positioned on the top of C−S−H layer and the whole system is optimized to compute the minimum energy of the system. This is followed by the MD simulation of the system under NVT ensemble at a temperature of 298 K for a period of 1 ps. The presence of Ca^{2+} ions causes the system to be charged. Therefore, we have used the Qeq method[32] to redistribute the overall charge on the atoms in the current atomistic model. After energy optimization of the cell, 120 ps of dynamic simulations with 1 fs time steps are carried out. This time period is long enough for the systems to reach convergence and energy stability. In this dynamic simulation, the charge is set to zero to eliminate the effect of charges resulting from the Ca^{2+} ions. Furthermore, in order to eliminate the effect of temperature on the adhesion, the simulations are carried out at room temperature. Polymers behave differently under different solvation conditions, especially in terms of the ions present in the system. However, the representative polymer systems studied here have no explicit solvent.

3. RESULTS AND DISCUSSION

3.1. Fiber/C−S−H Gel Interface Model. The complex atomistic model of C−S−H gel can be verified by important stoichiometric parameters such as C/S ratio and the first- and second-order thermodynamic quantities such as density and Young's modulus. All these parameters were explored in the previous section, and their agreement with the experimental model was confirmed. Another important factor that needs to be verified with available experimental data to make sure that the atomistic model is representative of the actual molecules is the radial distribution function (RDF). In a solid, the RDF has an infinite number of sharp peaks, of which the separations and heights are characteristic of the lattice structure.

The radial distribution functions of O−H, O−Ca, O−O, Si−Si, Ca−Ca, and Ca−Si pairs are shown in Figure 7. These results match precisely with the earlier NMR-investigated RDF graphs of C−S−H by Lequeux.[41] After verification of the model by the agreement between the presented parameters in our model and experimental data, the adhesion energies between the C−S−H model and PVA, polypropylene, and nylon-6 polymer fiber surface are investigated.

3.2. C−S−H/Polymer Interaction. The snapshots of the C−S−H/polymer model before and after the MD simulation for nylon-6, PVA, and polypropylene interfaces are shown in Figures 8, 9, 10, respectively. The binding energies between the C−S−H and polymers and the concentration profiles of the specific atoms are calculated after the MD simulations.

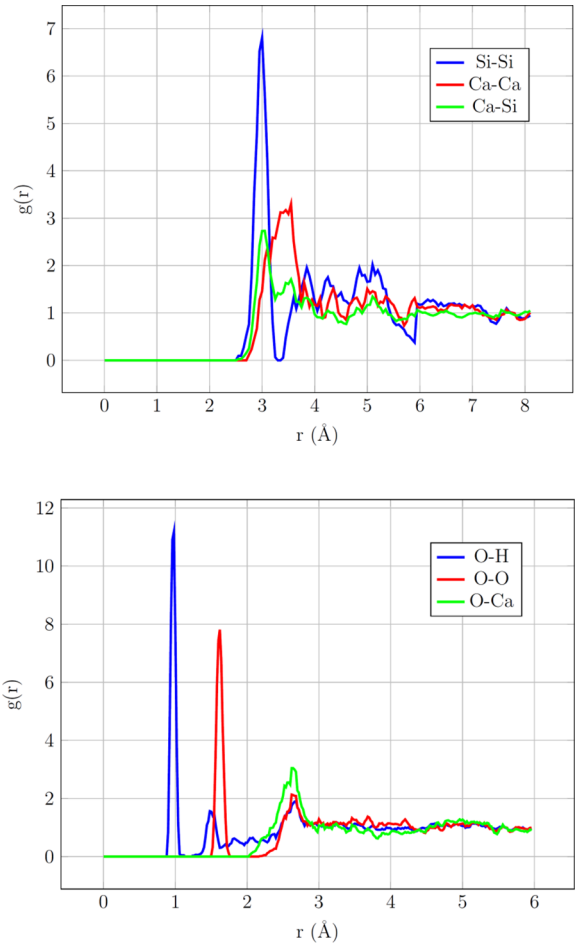

Figure 7. Radial distribution function of Si−Si, Ca−Ca, and Ca−Si pairs (top) and O−O, O−Ca, and O−H pairs (bottom) in C−S−H gel pairs in C−S−H gel.

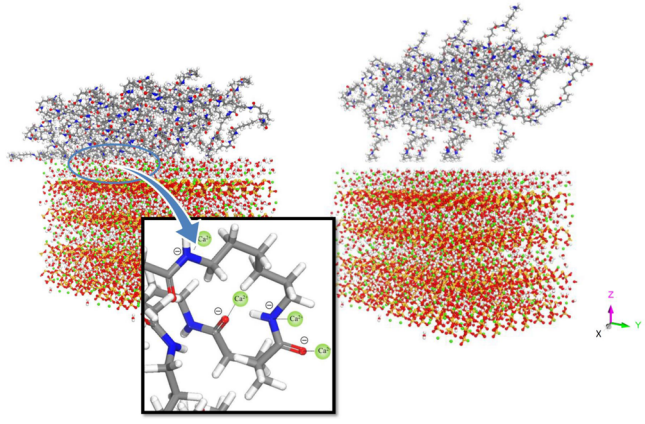

Figure 8. Nanostructure of nylon-6/C−S−H interface before, (right) and after simulation (left).

The interaction energy ($E_{\text{Interaction}}$) between the polymer molecules and the C−S−H surface is calculated by using the following equation:

$$E_{\text{interaction}} = (E_{\text{C-S-H}} + E_{\text{polymer}}) - E_{\text{total}} \quad (7)$$

where $E_{\text{interaction}}$ is the interaction energy of the system, E_{total} is the total energy of the C−S−H surface and the polymer molecules in equilibrium, $E_{\text{C-S-H}}$ is the energy of the surface

DOI: 10.1021/acsami.5b04344
ACS Appl. Mater. Interfaces 2015, 7, 17278−17286

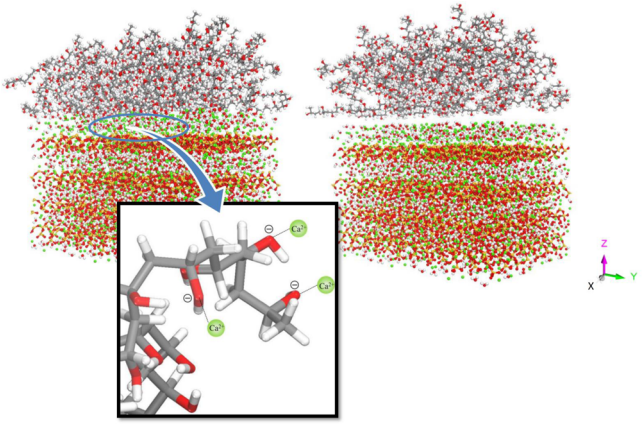

Figure 9. Nanostructure of PVA/C−S−H interface before, (right) and after simulation (left).

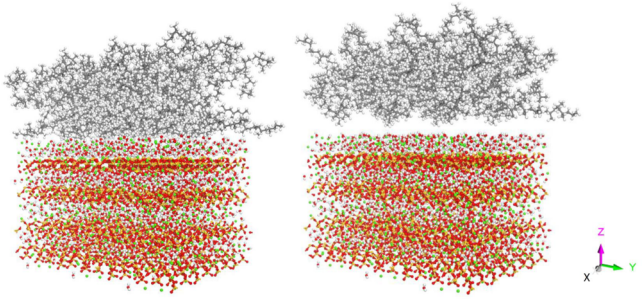

Figure 10. Nanostructure of polypropylene/C−S−H interface before (right) and after simulation (left).

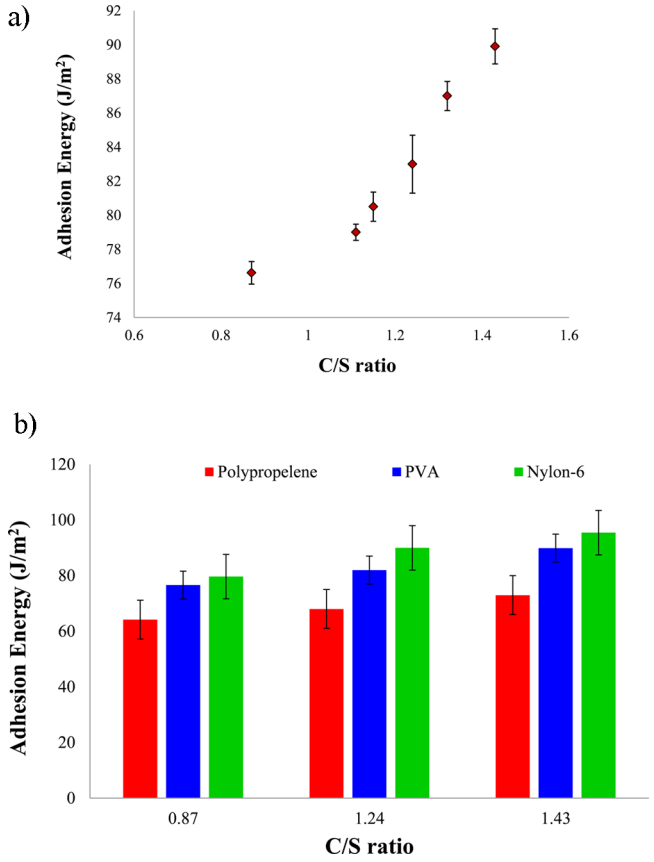

Figure 11. (a) Adhesion energies between PVA fiber and C−S−H gel as a function of interface C/S ratio; (b) Adhesion energies between polymers with different polarities with C−S−H as a function of interface C/S ratio.

without the polymer, and $E_{polymer}$ is the energy of the polymer without the surface both separated in vacuum in equilibrium.[42] These calculations are all single-point energies with no constraints defined in the model. To investigate the effect of polarity of fibers and C/S ratio on the adhesion energy of the fiber and cement, various atomistic simulation models are carried out. The results of the simulations for nylon-6, PVA, and polypropylene interfaces with C−S−H gel are presented in Figures 8, 9, 10, respectively. The accumulation of Ca^{2+} ions at the interface of nylon-6 and PVA can be observed in Figures 8 and 9, respectively.

To understand the effect of C/S ratio at the interface of C−S−H on the adhesion energy, the adhesion energy between C−S−H models with different C/S ratios with PVA fibers are investigated, and the results are presented in Figure 11a. These results clearly show that higher C/S ratios in C−S−H gel result in higher adhesion energies with PVA. This is mainly due to the existence of extra Ca^{2+} ions that make an electrostatic bond with the hydroxyl group of the fibers. This electrostatic bond is the origin of adhesion energy.

To understand the effect of polarity on the adhesion of matrix and fiber, the adhesion energies between the polymers and C−S−H models with different C/S ratios of 0.87, 1.24, and 1.43 are computed and are presented in Figure 11b. The results show that the adhesion energy increases as the polarity of the functional groups increases for each C/S ratio. The amide group is a high-polarity group having both oxygen and nitrogen sides in the functional group that can make hydrogen bonds and moreover interact with Ca^{2+}. The hydroxyl functional group has a mediocre polarity with one side that can interact with Ca^{2+} ion. Lastly, polypropylene does not have a polar functional group.

As shown by EDX analysis, the C/S ratio in C−S−H gel increases for polymer-fiber-reinforced concrete interfaces with polar fibers. The polarity of polymer fibers enhances the absorption of water molecules and the positive ions, such as Ca^{2+} dissolved during hardening, to the fiber molecules. Hence, the more realistic adhesion energy for each type of fiber-reinforced concrete can be calculated using the actual C/S ratio in C−S−H gel. The final interaction energies and the computed adhesion energies between PVA, polypropylene, and nylon-6 and relevant C−S−H gel models are presented in Table 4. Adhesion energy between PVA, polypropylene, and nylon-6 and C−S−H gel are computed as 89.91, 95.48, and 64.18 kJ/m^2, respectively. The variation in the computed adhesion energies is due to the presence of functional groups and hence different polarities of the polymer molecules. We believe that the functional groups affect the adhesion energy

Table 4. Contribution of Hydrogen Bonding, Electrostatic, and van der Waals Interaction Energies to the Total Adhesion Energy between Polymers and C−S−H gel

adhesion energy (J/m^2)	total energy	hydrogen bond	van der Waals	electrostatic
nylon-6	95.48	3.24	13.87	78.38
PVA	89.91	0.58	18.34	71.00
polypropylene	64.18	0.02	0.24	63.92

DOI: 10.1021/acsami.5b04344
ACS Appl. Mater. Interfaces 2015, 7, 17278−17286

primarily by changing the C/S ratio of the C−S−H at the interface and by absorbing additional positive ions in the C−S−H structure.

The contribution of hydrogen bonding, electrostatic, and van der Waals interaction energies to the total energy in the system are presented in Table 4. The results show that the adhesion energy between fibers and C−S−H gel is mostly a result of electrostatic interaction, which is due to the presence of Ca^{2+} ions in the C−S−H model. However, their strength increases with the induced polarity of the polymers. Additionally, the origin of the differences in the van der Waals bond strength is the permanent polarity of PVA and nylon-6 molecules. The difference in the hydrogen bond strength between C−S−H gel and fibers is that in the nylon-6 molecules both oxygen and nitrogen atoms contribute to the hydrogen bonding whereas in PVA molecules only one oxygen atom contributes to the hydrogen bonding and none of them exists in the polypropylene molecule to add to the adhesion energy.

4. CONCLUSIONS

Across the globe, polymer fibers are added to concrete to enhance the tensile properties and ductility of concrete. Although there is a large body of data on this subject, the nanostructure and nanomechanical properties of polymer fiber/cement interface is still not completely known, which is pivotal in the design of robust polymer-reinforced concrete. This study presents a combined SEM/EDX analysis and atomistic simulation framework to investigate the nanostructure of the cement/fiber interfaces, and the corresponding mechanical properties. In this study, different polymer fibers are used on the basis of different polarity of their functional group. The electron microscopy results show the ratio of C/S changes in the fiber/matrix interface for the three types of polymer fibers studied. This is essentially due to the different polarities of the polymer molecules. Using SEM/EDX analysis, it is shown that the C/S ratios in PVA/C−S−H and nylon-6/C−S−H interfaces are higher than that in polypropylene/C−S−H interface. This is mainly a result of the high polarity of hydroxyl and amide functional groups. To further investigate this hypothesis, using the proposed atomistic model, the adhesion energies between different polymers and C−S−H are computed. It is observed that the functional group affects the adhesion energy primarily by changing the C/S ratio of the C−S−H at the interface and by absorbing additional positive ions in the C−S−H structure. The implications of these results are significant in further development of robust fiber-reinforced cement composites. Future work will focus on understanding the rate of migration of calcium atoms at the surface/interface.

AUTHOR INFORMATION

Corresponding Author

*E-mail: nrahbar@wpi.edu.

Notes

The authors declare no competing financial interest.

ACKNOWLEDGMENTS

The project is partially supported by NSF CAREER grant no. 1261284 and by N.R.'s WPI start-up grant.

REFERENCES

(1) Balaguru, P. N.; Shah, S. P. *Fiber-reinforced Cement Composites*; McGraw-Hill: New York, 1992.

(2) Sakulich, A. R. Reinforced Geopolymer Composites for Enhanced Material Greenness and Durability. *Sustain. Cities Society* **2011**, *1*, 195−210.

(3) Sharifi N. P., Sakulich A. Application of Phase Change Materials in Structures and Pavements. In *Proceedings of the 2nd International Workshop on Design in Civil and Environmental Engineering*, Worchester, Massachusetts, June 28−29, 2013; Thompson, M. K., Ed.; DCEE: Worchester, MA, 2013; pp 82−88

(4) Sharifi, N. P.; Sakulich, A. Application of Phase Change Materials to Improve the Thermal Performance of Cementitious Material. *Energy Buildings* **2015**, *103*, 83−95.

(5) Akihama, S.; Suenaga, T.; Nakagawa, H.; Suzuki, K. Experimental Study of Vinylon Fiber Reinforced Cement Composites. VFRC (Part I). In *Kajima Annual Technical Report*; Kajima Corporation: Tokyo, Japan, 1985; Vol. 33, pp 123−128.

(6) Garcia, S.; Naaman, A. E.; Pera, J. Experimental Investigation on the Potential Use of Poly (vinyl alcohol) Short Fibers in Fiber-reinforced Cement-based Composites. *Mater. Constr.* **1997**, *30*, 43−52.

(7) Betterman, L.; Ouyang, C.; Shah, S. Fiber-matrix Interaction in Microfiber-reinforced Mortar. *Adv. Cem. Based Mater.* **1995**, *2*, 53−61.

(8) Li, V. C.; Chan, Y.-W.; Wu, H.-C. Interface Strengthening Mechanisms in Polymeric Fiber reinforced Cementitious Composites. *Brittle Matrix Compos. 4, [Proc. Int. Symp.], 4th*; abstract no. 41994.

(9) *Global Cement Report*, 9th ed.; International Cement Review; London, 2011.

(10) Van Vliet, K.; Pellenq, R.; Buehler, M. J.; Grossman, J. C.; Jennings, H.; Ulm, F. J.; Yip, S. Set in Stone? A Perspective on the Concrete Sustainability Challenge. *MRS Bull.* **2012**, *37*, 395−402.

(11) Bentur, A.; Mindess, S. *Fibre Reinforced Cementitious Composites*, 2nd ed.; Taylor & Francis: London, 2007.

(12) Sakulich, A. R.; Li, V. C. Nanoscale Characterization of Engineered Cementitious Composites (ECC). *Cem. Concr. Res.* **2011**, *41*, 169−175.

(13) Dolado, J. S.; Griebel, M.; Hamaekers, J. A Molecular Dynamic Study of Cementitious Calcium Silicate Hydrate (C−S−H) gels. *J. Am. Ceram. Soc.* **2007**, *90*, 3938−3942.

(14) Yu, P.; Kirkpatrick, R. J.; Poe, B.; McMillan, P. F.; Cong, X. Structure of Calcium Silicate Hydrate (C-S-H): Near-, Mid-, and Far-infrared Spectroscopy. *J. Am. Ceram. Soc.* **1999**, *82*, 742−748.

(15) Soyer-Uzun, S.; Chae, S. R.; Benmore, C. J.; Wenk, H. R.; Monteiro, P. J. Compositional Evolution of Calcium Silicate Hydrate (C−S−H) Structures by Total X-ray Scattering. *J. Am. Ceram. Soc.* **2012**, *95*, 793−798.

(16) Allen, A. J.; Thomas, J. J.; Jennings, H. M. Composition and Density of Nanoscale Calcium−Silicate−Hydrate in Cement. *Nat. Mater.* **2007**, *6*, 311−316.

(17) Hamid, S. The Crystal Structure of the 11 Å Natural Tobermorite Ca2. 25 [Si3O7. 5 (OH) 1.5]·1H2O. *Z. Kristallogr. - Cryst. Mater.* **1981**, *154*, 189−198.

(18) Taylor, H. Nanostructure of C-S-H: Current Status. *Adv. Cem. Based Mater.* **1993**, *1*, 38−46.

(19) Shahsavari, R.; Pellenq, RJ-M; Ulm, F.-J. Empirical Force Fields for Complex Hydrated Calcio-silicate Layered Materials. *Phys. Chem. Chem. Phys.* **2011**, *13*, 1002−1011.

(20) Pellenq, R.-M.; Lequeux, N.; Van Damme, H. Engineering the Bonding Scheme in C−S−H: The Iono-covalent Framework. *Cem. Concr. Res.* **2008**, *38*, 159−174.

(21) Richardson, I. The Calcium Silicate Hydrates. *Cem. Concr. Res.* **2008**, *38*, 137−158.

(22) Wu, W.; Al-Ostaz, A.; Cheng, AH-D; Song, C. R. Computation of Elastic Properties of Portland Cement Using Molecular Dynamics. *J. Nanomechanics Micromechanics* **2011**, *1*, 84−90.

(23) Richardson, I. Tobermorite/Jennite-and Tobermorite/Calcium Hydroxide-Based Models for The Structure of CSH: Applicability to Hardened Pastes of Tricalcium Silicate, B-Dicalcium Silicate, Portland Cement, and Blends of Portland Cement with Blast-Furnace Slag, Metakaolin, or Silica Fume. *Cem. Concr. Res.* **2004**, *34*, 1733−1777.

DOI: 10.1021/acsami.5b04344
ACS Appl. Mater. Interfaces 2015, 7, 17278−17286

(24) Bauchy, M.; Qomi, M. A.; Ulm, F.-J.; Pellenq, R.-M. Order and Disorder in Calcium−Silicate−Hydrate. *J. Chem. Phys.* **2014**, *140*, 214503.
(25) Pellenq, RJ-M; Kushima, A.; Shahsavari, R.; Van Vliet, K. J.; Buehler, M. J.; Yip, S.; Ulm, F. J. A Realistic Molecular Model of Cement Hydrates. *Proc. Natl. Acad. Sci. U. S. A.* **2009**, *106*, 16102−16107.
(26) Abdolhosseini Qomi, M.; Krakowiak, K.; Bauchy, M.; Stewart, K. L.; Shahsavari, R.; Jagannathan, D.; Brommer, D. B.; Baronnet, A.; Buehler, M. J.; Yip, S.; Ulm, F. J.; Van Vliet, K. J.; Pellenq, R. J. M. Combinatorial Molecular Optimization of Cement Hydrates. *Nat. Commun.* **2014**, *5*, 4960.
(27) McNaught, A. D., Wilkinson, A., Eds.*Compendium of Chemical Terminology*, 2nd ed.; Royal Society of Chemistry: London, 1997.
(28) Sun, H. COMPASS: An Ab Initio Force-Field Optimized for Condensed-Phase Applications Overview with Details on Alkane and Benzene Compounds. *J. Phys. Chem. B* **1998**, *102*, 7338−7364.
(29) Sun, H.; Ren, P.; Fried, J. The COMPASS Force Field: Parameterization and Validation for Phosphazenes. *Comput. Theor. Polym. Sci.* **1998**, *8*, 229−246.
(30) Grujicic, M.; Sun, Y.-P.; Koudela, K. The Effect of Covalent Functionalization of Carbon Nanotube Reinforcements on The Atomic-Level Mechanical Properties of Poly-Vinyl-Ester-Epoxy. *Appl. Surf. Sci.* **2007**, *253*, 3009−3021.
(31) Lu, Z.; Dunn, M. L. Van der Waals Adhesion of Graphene Membranes. *J. Appl. Phys.* **2010**, *107*, 044301.
(32) Rappe, A. K.; Goddard, W. A., III Charge Equilibration for Molecular Dynamics Simulations. *J. Phys. Chem.* **1991**, *95*, 3358−3363.
(33) Manzano, H.; Dolado, J.; Ayuela, A. Elastic Properties of the Main Species Present in Portland Cement Pastes. *Acta Mater.* **2009**, *57*, 1666−1674.
(34) Manzano, H.; Dolado, J.; Guerrero, A.; Ayuela, A. Mechanical Properties of Crystalline Calcium-Silicate-Hydrates: Comparison with Cementitious C-S-H Gels. *Phys. Status Solidi A* **2007**, *204*, 1775−1780.
(35) Constantinides, G.; Ulm, F.-J. The Effect Of Two Types of CSH on the Elasticity of Cement-Based Materials: Results from Nanoindentation and Micromechanical Modeling. *Cem. Concr. Res.* **2004**, *34*, 67−80.
(36) Gujrati, P. D., Leonov, A. I., Eds. *Modeling and Simulation in Polymers*; John Wiley & Sons: Weinheim, Germany, 2010.
(37) Cranford, S. W.; Ortiz, C.; Buehler, M. J. Mechanomutable Properties of a PAA/PAH Polyelectrolyte Complex: Rate Dependence and Ionization Effects on Tunable Adhesion Strength. *Soft Matter* **2010**, *6*, 4175−4188.
(38) Hossain, D.; Tschopp, M.; Ward, D.; Bouvard, J.; Wang, P.; Horstemeyer, M. Molecular Dynamics Simulations of Deformation Mechanisms of Amorphous Polyethylene. *Polymer* **2010**, *51*, 6071−6083.
(39) Debenedetti, P. G.; Stillinger, F. H. Supercooled Liquids and the Glass Transition. *Nature* **2001**, *410*, 259−267.
(40) Capaldi, F. M.; Boyce, M. C.; Rutledge, G. C. Molecular Response of a Glassy Polymer to Active Deformation. *Polymer* **2004**, *45*, 1391−1399.
(41) Lequeux, N.; Morau, A.; Philippot, S.; Boch, P. Extended X-ray Absorption Fine Structure Investigation of Calcium Silicate Hydrates. *J. Am. Ceram. Soc.* **1999**, *82*, 1299−1306.
(42) Kisin, S.; Bozovic Vukic, J.; van der Varst, P. G. T.; de With, G.; Koning, C. E. Estimating the Polymer-Metal Work of Adhesion from Molecular Dynamics Simulations. *Chem. Mater.* **2007**, *19*, 903−907.
(43) Askeland, D. R.; Phulé, P. P. *The Science and Engineering of Materials*, 4th ed.; Brooks/Cole-Thomson Learning: Monterey, CA, 2003.
(44) Rachtanapun, P.; Selke, S. E.; Matuana, L. M. Relationship Between Cell Morphology and Impact Strength of Microcellular Foamed High-Density Polyethylene/Polypropylene Blends. *Polym. Eng. Sci.* **2004**, *44*, 1551−1560.
(45) Liu, H.; Wu, Q.; Zhang, Q. Preparation and Properties of Banana Fiber-Reinforced Composites Based on High Density Polyethylene (HDPE)/Nylon-6 Blends. *Bioresour. Technol.* **2009**, *100*, 6088−6097.
(46) Pakzad, A.; Simonsen, J.; Yassar, R. S. Elastic Properties of Thin Poly (Vinyl Alcohol)−Cellulose Nanocrystal Membranes. *Nanotechnology* **2012**, *23*, 085706.
(47) Svoboda, P.; Theravalappil, R.; Svobodova, D.; Mokrejs, P.; Kolomaznik, K.; Mori, Kiesuke; Ougizawa, T.; Inoue, T. Elastic Properties of Polypropylene/Ethylene−Octene Copolymer Blends. *Polym. Test.* **2010**, *29*, 742−748.
(48) Fornes, T.; Yoon, P.; Keskkula, H.; Paul, D. Nylon 6 Nanocomposites: the Effect of Matrix Molecular Weight. *Polymer* **2001**, *42*, 09929−09940.
(49) Liu, T.; Phang, I. Y.; Shen, L.; Chow, S. Y.; Zhang, W.-D. Morphology and Mechanical Properties of Multiwalled Carbon Nanotubes Reinforced Nylon-6 Composites. *Macromolecules* **2004**, *37*, 7214−7222.
(50) Finch, C. A., Ed. *Polyvinyl alcohol: Developments*; Wiley: Chichester, 1992.

DOI: 10.1021/acsami.5b04344
ACS Appl. Mater. Interfaces 2015, 7, 17278−17286